IOPscience iopscience.iop.org

Home Search Collections Journals About Contact us My IOPscience

All-temperature magnon theory of ferromagnetism

This article has been downloaded from IOPscience. Please scroll down to see the full text article.

2009 J. Phys.: Condens. Matter 21 336003

(http://iopscience.iop.org/0953-8984/21/33/336003)

View the table of contents for this issue, or go to the journal homepage for more

Download details:
IP Address: 129.252.86.83
The article was downloaded on 29/05/2010 at 20:45

Please note that terms and conditions apply.

J. Phys.: Condens. Matter **21** (2009) 336003 (14pp) doi:10.1088/0953-8984/21/33/336003

All-temperature magnon theory of ferromagnetism

Sambhu N Datta and Anirban Panda

Department of Chemistry, Indian Institute of Technology–Bombay, Powai, Mumbai-400076, India

E-mail: sndatta@chem.iitb.ac.in and anirban@chem.iitb.ac.in

Received 23 March 2009, in final form 23 June 2009
Published 24 July 2009
Online at stacks.iop.org/JPhysCM/21/336003

Abstract

We present an all-temperature magnon formalism for ferromagnetic solids. To our knowledge, this is the first time that all-temperature spin statistics have been calculated. The general impression up to now is that the magnon formalism breaks down at the Curie point as it introduces a series expansion and unphysical states. Our treatment is based on an accurate quantum mechanical representation of the Holstein–Primakoff transformation. To achieve this end, we introduce the 'Kubo operator'. The treatment is valid for all 14 types of Bravais lattices, and not limited to simple cubic unit cells. In the present work, we carry out a zeroth-order treatment involving all possible spin states, and leaving out all unphysical states. In a subsequent paper we will show that the perturbed energy values are very different, but the magnetic properties undergo only small modifications from the zeroth-order results.

(Some figures in this article are in colour only in the electronic version)

1. Introduction

A reliable theoretical treatment of ferromagnetic (FM) solids is based on the so-called magnon formalism that represents the standard quantum statistical field theory of these systems. The magnon theory, however, has its own limitations. The theory is based upon the Holstein–Primakoff transformation [1] which contains a square root term and its series expansion loses rapid convergence with the rise in temperature. It is also associated with infinitely many bosonic states, most of which are unphysical, and it breaks down as soon as the temperature crosses the Curie point. The saving grace for the ferromagnetic spin wave approximation is that the ground state of the Heisenberg model is still treated exactly, because the presumed vacuum is in fact the ground state configuration. The classical behavior is reached at a much higher temperature where $z\boldsymbol{J}/k_{\mathrm{B}}T \ll 1$, z being the number of nearest neighbors and $\boldsymbol{J}$ the exchange coupling constant between two adjacent units.

A large body of work has been carried out by different authors on this subject, but these are mostly on the Heisenberg one-dimensional chain and the Ising model [2]. Although popular in the literature, the latter models involve Hamiltonian operators that are obtained by truncating the full spin Hamiltonian rather drastically, thereby achieving mathematical simplicity [3a, 3b, 3c, 3d, 3e]. To get a better solution at different temperatures, some authors have resorted to numerical calculations on extremely small systems [4a, 4b, 4c, 4d, 4e]. Several authors have also investigated the possibility of bound states of magnons that are revealed at the Brillouin zone boundary, when the crystal has anisotropy [5a, 5b, 5c, 5d, 5e, 5f, 5g, 5h, 5i]. Reser and Melnikov investigated the problem of temperature dependence of strong ferromagnets using dynamic spin-fluctuation theory [5j]. Using the polarized neutron diffraction method Cable has experimentally established that there exits an asymmetry in the unpaired spin density of Ni in e_g and t_{2g} subbands [2i]. However, a completely novel approach is needed to understand ferromagnetism in a *three-dimensional* crystal at *all ranges* of temperature. Accurate spin state statistics are required for this purpose.

There is an asymmetry involved in the conventional treatment of magnons, where the statistical mechanical averaging is done by assuming one-magnon states [6] and then the effect of magnon–magnon interaction is evaluated. In the absence of a magnetic field, there is no preferred z-axis. The ferromagnetic domain structure and the random distribution of the spin axes of the domains in the absence of a magnetic field are well known. A FM microcrystal must have the same internal energy per unit species in the absence of a field when it is inverted, or rotated in any other orientation. This implies

 © 2009 IOP Publishing Ltd Printed in the UK

that for a given z-axis, a specific n-magnon state and the complementary $(N - n)$-magnon state must have the same energy. This is not so in the conventional one-magnon picture where one uses a specific z-axis, and differently oriented domains would have different energy per unit species. In this series of works we pay special attention to retaining the orientational symmetry in the field-free case.

We put forward a magnon treatment of ferromagnetic solids avoiding the series expansion of a square root, and using the magnon–magnon interaction in an exact form. Moreover, we carry out each sum over the finite number of physical magnon states, and not over an infinite number. In this way we avoid the unphysical states, and the analysis becomes valid for all ranges of temperature. The theory we describe deals in principle with the full magnon–magnon interaction, although its effect will be considered here up to the first order as the higher-order contributions are estimated to be quite small. We show that the energy and the population distribution of the various magnon states exceptionally differ from those in the conventional one-magnon picture, but the final expressions for the physical properties remain comparable. Besides, we interpret the so-called molecular field and describe it as a function of temperature. The present paper (paper I) gives the mathematical basis of our treatment and the zeroth-order results. In a subsequent article (paper II, [7]) we discuss the perturbed system and compare our analysis with that of Dyson for a temperature close to the Curie point. The concept of a spin wave is not necessarily limited to a low temperature domain, and field theory needs to be carefully implemented while the coupling is not so weak.

2. Hamiltonian

2.1. Traditional Hamiltonian

The simplest Hamiltonian of interest in the presence of an external magnetic field of strength B is the so-called nearest-neighbor Heisenberg exchange Hamiltonian described by

$$H = -g\mu_{\mathrm{B}}B\sum_j S_{jz} - \sum_{j,\varepsilon,\delta} J_\varepsilon \boldsymbol{S}_j \cdot \boldsymbol{S}_{j+\delta_\varepsilon} \tag{1}$$

where g is gyromagnetic ratio, $\mu_{\mathrm{B}}(=e_0\hbar/2m_ec)$ is the Bohr magneton, j indicates the lattice sites, and the vector δ_ε is the connectivity vector for two nearest neighbors in the ε direction as shown in figure 1. The constant J_ε is known as the exchange coupling constant along direction ε, and $\boldsymbol{S}_j$ is the spin angular momentum operator at site j. In practice, the Hamiltonian for ferromagnetic solids is written in terms of Bose operators of type a_j and $a_j^\dagger$ that are obtained from spin operators (S_j^+ and S_j^-) by the Holstein–Primakoff transformation [1]

$$S_j^+ = (2S)^{1/2} f(\hat{n}_j) a_j, \qquad S_j^- = (2S)^{1/2} a_j^\dagger f(\hat{n}_j). \tag{2}$$

In the above, $f(\hat{n}_j) = (1 - \hat{n}_j/2S)^{1/2}$ and $\hat{n}_j = a_j^\dagger a_j$. The Holstein–Primakoff transformation is nonlinear and has not traditionally been amenable to exact calculations. In particular, $S_{jz} = S - \hat{n}_j$, such that $\hat{n}_j$ is the number operator for the spin excitations at site j. The operators a_j and $a_j^\dagger$ are the corresponding destruction and creation operators for the spin excitations. This leads to the exchange Hamiltonian

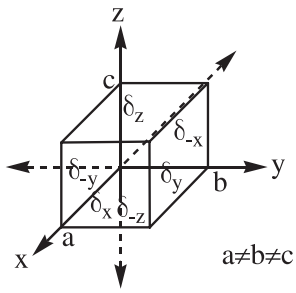

Figure 1. The connectivity vector (δ) for nearest neighbors along the axes of an orthogonal crystal.

$$\begin{aligned} H = {} & -g\mu_{\mathrm{B}}BNS - 2NS^2\sum_\varepsilon J_\varepsilon \\ & + \left\{ g\mu_{\mathrm{B}}B + 4S\left(\sum_\varepsilon J_\varepsilon\right)\right\}\sum_j \hat{n}_j \\ & - S\sum_j\sum_\varepsilon J_\varepsilon \sum_{\delta_\varepsilon}\{f(\hat{n}_j)a_j a_{j+\delta_\varepsilon}^\dagger f(\hat{n}_{j+\delta_\varepsilon}) \\ & + a_j^\dagger f(\hat{n}_j) f(\hat{n}_{j+\delta_\varepsilon}) a_{j+\delta_\varepsilon}\} \\ & - \sum_j\sum_\varepsilon J_\varepsilon \sum_{\delta_\varepsilon} \hat{n}_j \hat{n}_{j+\delta_\varepsilon} \end{aligned} \tag{3}$$

where N is the total number of lattice sites.

2.2. Limitations

Fourier transformations of the operators a_j and $a_j^\dagger$ give magnon operators b_k and $b_k^\dagger$:

$$\begin{aligned} b_{\boldsymbol{k}} &= N^{-1/2}\sum_j \mathrm{e}^{\mathrm{i}\boldsymbol{k}\cdot\boldsymbol{r}_j} a_j, \\ b_{\boldsymbol{k}}^\dagger &= N^{-1/2}\sum_j \mathrm{e}^{-\mathrm{i}\boldsymbol{k}\cdot\boldsymbol{r}_j} a_j^\dagger. \end{aligned} \tag{4}$$

Since the latter are also Bose operators, they are associated with an infinite number of states, most of which are unphysical. Any Hamiltonian written in terms of the magnon operators would involve the problem of mixing of these unphysical states in the treatment. The actual problem starts from the site operator $a_j^\dagger$. While $S_j^-|-S\rangle = 0$ that indicates a maximum of $2S$ excitations per site, $a_j^\dagger|n_j = 2S\rangle \neq 0$. In reality, a finite number of states should be involved in expression (3), because $f(\hat{n}_j)|n_j = 2S\rangle = 0$. The number of spin states is $(2S+1)^N$. This requires an accurate handling of the operator $f(\hat{n}_j)$ in equation (3). Another difficulty arises from this requirement. It is normal to expand the operator $f(\hat{n}_j)$ as a square root. This expansion is infinitely large and needs to be truncated in practice. The truncation works only if $n_j/2S \ll 1$, that is, at an extremely low temperature. As a matter of fact, the conventional magnon treatment is known to break down as soon as the temperature crosses the Curie point (FM) [6], because of the increasing truncation error and a large population of the unphysical states at a higher

Table 1. The number of states for small N values. Not all the magnon states are physically acceptable.

	$S = 1/2$		$S = 1$		$S = 3/2$	
N	Site states	Magnon states	Site states	Magnon states	Site states	Magnon states
1	2	2	3	3	4	4
2	4	6	9	15	16	28
3	8	20	27	84	64	220
4	16	70	81	495	256	1820

temperature. In passing, we mention that Bloch has shown magnon renormalization to be necessary near the Curie point in ferromagnets [8].

2.3. Physical states

The site spin states are written as $\prod_j |n_j\rangle$ such that $\sum_j n_j = n_{\rm tot}$, $0 \leqslant n_j \leqslant 2S$ for each j. There are $N\boldsymbol{k}$ values, and all the $\boldsymbol{k}$ states are *a priori* equally probable. It is easy to show that $\sum_{\boldsymbol{k}} n_{\boldsymbol{k}} = \sum_j n_j$ and the $n_{\boldsymbol{k}}$ values are limited as

$$n_{\boldsymbol{k}} = 0, 1, \ldots, n_{\rm tot} \tag{5}$$

for all $\boldsymbol{k}$ subject to the constraint that the total number of excitations is less than or equal to $2NS$:

$$n_{\rm tot} = \sum_{\boldsymbol{k}} n_{\boldsymbol{k}} = 0, 1, \ldots, 2NS. \tag{6}$$

The above consideration generates a total of $N_{\rm mag} = {}^{(2S+1)N}C_N$ magnon states. Basically this means that $(2S+1)N$ primitive magnon functions (site states) are distributed among N magnon modes. The number $N_{\rm mag}$ is large yet finite. The numbers of primitive (site) states and magnon states are given for various S in table 1.

However, not all of the magnon states are physically acceptable, as $(2S+1)^N$ site states can linearly combine to form the same number of orthonormal magnon states. This hints that the $n_{\boldsymbol{k}}$ values should be limited as $n_{\boldsymbol{k}} = 0, 1, \ldots, \min[2S, n_{\rm tot}]$. In appendix A we show that the physically acceptable magnon states can be formed from states like $|n_{\boldsymbol{k}}\rangle$ with $0 \leqslant n_{\boldsymbol{k}} \leqslant 2S$.

2.4. The Kubo operator

In order to avoid the truncation error by treating the operator $f(\hat{n}_j)$ in an exact manner, we rediscover a technique that was employed by Kubo [9] but has remained largely overlooked. Kubo showed that a finite expression of the function $f(n_j)$ can be obtained by expanding it as a polynomial of degree m:

$$f(n_j) \equiv (1 - n_j/2S)^{1/2} = P^m(n_j), \tag{7}$$

that is to be valid for $n_j = 0, 1, \ldots, 2S$. This is uniquely satisfied if $m = 2S$, that is

$$f(n_j) \equiv P^{(2S)}(n_j) = \sum_{i=0}^{2S} f_i n_j^i. \tag{8}$$

The coefficients f_i were determined for different S values by Kubo [9a]. Some of the Kubo coefficients are given in table 2.

Since the eigenvalue of $\hat{n}$ is n, one can use the *operator equivalence*

$$f(\hat{n}_j) = \sum_{i=0}^{2S} f_i \hat{n}_j^i. \tag{9}$$

This expression strictly limits the accessible primitive states to $|n_j = 0\rangle, \ldots, |n_j = 2S\rangle$, as

$$\sum_{i=0}^{2S} f_i \hat{n}_j^i |n_j = 2S\rangle = f(2S)|2S\rangle = 0. \tag{10}$$

Consequently, the theoretical treatment would be limited to $(2S+1)^N$ primitive microstates. Henceforth in this work the operators $f(\hat{n}_j)$ will called Kubo operators.

2.5. Physically relevant Hamiltonian

We consider a crystal where each species in the bulk has z nearest neighbors. Because of translational symmetry $\bar{J}_{\boldsymbol{k}-\boldsymbol{l}} = \bar{J}_{\boldsymbol{l}-\boldsymbol{k}}$, where $\bar{J}_{\boldsymbol{k}} = z^{-1}\sum_\varepsilon J_\varepsilon \gamma_{\boldsymbol{k}\varepsilon}$, and $\gamma_{\boldsymbol{k}\varepsilon} = \sum_{\delta_\varepsilon} {\rm e}^{{\rm i}\boldsymbol{k}\cdot\delta_\varepsilon}$. We will use the quantities $\omega_{\boldsymbol{k}} = \omega_0' - \omega_{\boldsymbol{k}}'$, $\omega_0' = 2zS\bar{J}$, $\bar{J} = 2z^{-1}\sum_\varepsilon J_\varepsilon$, and $\omega_{\boldsymbol{k}}' = 2zS\bar{J}_{\boldsymbol{k}} = \omega_{-\boldsymbol{k}}'$. When the expression for the Kubo operator is used in equation (3) and the site boson operators are converted into the magnon operators, the Hamiltonian for a ferromagnet appears as $H = H^{(0)} + H'$ where the zeroth-order operator is for 'non-interacting' magnons,

$$H^{(0)} = -g\mu_{\rm B}NSB - zNS^2\bar{J} + g\mu_{\rm B}B\sum_{\boldsymbol{k}}\hat{n}_{\boldsymbol{k}} + \sum_{\boldsymbol{k}}\hat{n}_{\boldsymbol{k}}\omega_{\boldsymbol{k}}, \tag{11}$$

and the magnon–magnon interaction constitutes the perturbation

$$\begin{aligned} H' = &-\sum_{\boldsymbol{k},\boldsymbol{l},\boldsymbol{m}}\left\{\frac{f_1}{N}(\omega_{\boldsymbol{k}}' + \omega_{\boldsymbol{l}}') + \frac{1}{2NS}\omega_{\boldsymbol{k}-\boldsymbol{l}}'\right\} b_{\boldsymbol{k}}^\dagger b_{\boldsymbol{m}}^\dagger b_{\boldsymbol{l}} b_{\boldsymbol{k}-\boldsymbol{l}+\boldsymbol{m}} \\ &- \frac{1}{2}\sum_{p,q=1}^{2S}\frac{f_p f_q}{N^{p+q}}\sum_{\substack{\boldsymbol{k}_1,\ldots,\boldsymbol{k}_p \\ \boldsymbol{l}_1,\ldots,\boldsymbol{l}_q}}\sum_{\substack{\boldsymbol{k}_1',\ldots,\boldsymbol{k}_p' \\ \boldsymbol{l}_1',\ldots,\boldsymbol{l}_q'}} \\ &\times \sum_{\boldsymbol{m}}\{\omega'_{\boldsymbol{m}-\sum(\boldsymbol{k}-\boldsymbol{l})} b_{\boldsymbol{k}_1}^\dagger b_{\boldsymbol{l}_1}\cdots b_{\boldsymbol{k}_p}^\dagger b_{\boldsymbol{l}_p} b_{\boldsymbol{m}} \\ &\times b^\dagger_{\boldsymbol{m}-\sum(\boldsymbol{k}-\boldsymbol{l})-\sum(\boldsymbol{k}'-\boldsymbol{l}')} b_{\boldsymbol{k}_1'}^\dagger b_{\boldsymbol{l}_1'}\cdots b_{\boldsymbol{k}_q'}^\dagger b_{\boldsymbol{l}_q'} \\ &+ \omega'_{\boldsymbol{m}+\sum(\boldsymbol{k}-\boldsymbol{l}')} b_{\boldsymbol{m}}^\dagger b_{\boldsymbol{k}_1}^\dagger b_{\boldsymbol{l}_1}\cdots b_{\boldsymbol{k}_p}^\dagger b_{\boldsymbol{l}_p} b_{\boldsymbol{k}_1'}^\dagger b_{\boldsymbol{l}_1'}\cdots \\ &\times b_{\boldsymbol{k}_q'}^\dagger b_{\boldsymbol{l}_q'} b_{\boldsymbol{m}+\sum(\boldsymbol{k}-\boldsymbol{l})+\sum(\boldsymbol{k}'-\boldsymbol{l}')}\}. \end{aligned} \tag{12}$$

A comparison with the traditional Hamiltonian is due here. The conventional treatment yields the same $H^{(0)}$ but $H'_{\rm conv}$ as an expansion up to, say, the biquadratic terms [6]:

$$H'_{\rm conv} = \frac{1}{4NS}\sum_{\boldsymbol{k},\boldsymbol{l},\boldsymbol{m}}(\omega_{\boldsymbol{k}}' + \omega_{\boldsymbol{l}}' - 2\omega_{\boldsymbol{k}-\boldsymbol{l}}')b_{\boldsymbol{k}}^\dagger b_{\boldsymbol{m}}^\dagger b_{\boldsymbol{l}} b_{\boldsymbol{k}-\boldsymbol{l}+\boldsymbol{m}}. \tag{13}$$

Because of the square root expansion, the coefficient $-1/4S$ takes the place of f_1. Other higher-order terms similarly occur with the appropriate coefficients calculated from the square root expansion, but these are traditionally neglected. The

Table 2. Kubo coefficients.

S	f_0	f_1	f_2	f_3
1/2	1	-1		
1	1	$-(3/2-\sqrt{2})$	$-(\sqrt{2}-1)/2$	
3/2	1	$-(11+3\sqrt{3}-6\sqrt{6})/6$	$(6+4\sqrt{3}-5\sqrt{6})/6$	$(-1-\sqrt{3}+\sqrt{6})/6$

conventional treatment contains an infinity of orders of $b^\dagger b$. It is transparent that the operator H' in equation (12) contains spin wave coupling contributions only up to $4S$ biquadratic terms. The perturbation H' contains both diagonal and off-diagonal terms. The diagonal terms give rise to the first-order energy correction.

The diagonal terms in the conventional Hamiltonian have been considered in a self-consistent formalism by Dyson [10]. Dyson, however, used non-orthogonal basic states that are built from the effect of $a_j^\dagger f(\hat{n}_j)$ operators. At low temperatures, the only important basic states are approximately orthogonal to each other, and the effective Hamiltonian becomes almost diagonal. Dyson found that the residual interaction is only dynamical which makes the situation superficially simpler. He worked with a modified Hamiltonian in the 'ideal' Hilbert space. The off-diagonal terms contribute to higher orders. The higher-order energy corrections were estimated by Dyson. His treatment generated a complete description of the thermodynamic properties of the system, but in the low temperature region, around and below the Curie point. Our objective here is to describe the thermodynamic properties at all ranges of temperature.

2.6. Energy contributions

The zeroth-order energy for a specific magnon state is given by

$$E^{(0)} = -g\mu_B NSB - zNS^2\bar{J} + g\mu_B B\sum_k n_k + \sum_k n_k\omega_k. \tag{14}$$

The magnon–magnon interaction terms consist of diagonal as well as off-diagonal contributions. The diagonal contributions contribute to the first-order energy correction, while the off-diagonal terms can be used to determine the higher-order corrections to energy. The higher-order contributions are at most of order $1/N$. Therefore, the higher-order corrections can be safely neglected as $N \to \infty$, and the total energy will be mainly composed of the zeroth-order and the first-order contributions.

Henceforth in this work we will write n instead of $n_{\rm tot}$.

It can be easily shown that for $B = 0$ and for the 'site states' given by (A.1) and (A.2) for $S = 1/2$ in appendix A,

$$\langle H\rangle_n = \langle H\rangle_{N-n} = -zN\bar{J}S^2 + \frac{n(N-n)}{N}\omega_0' - \frac{1}{N}\sum_{k\neq 0}\left|\sum_{s=1}^{n} e^{-ik\cdot s}\right|^2\omega_k'. \tag{15}$$

That is, in the absence of an external magnetic field, the energy corresponding to the states with n and $(N-n)$ site excitations should be the same, thereby demonstrating that there is no preference for the z-axis.

A difference between $\langle H\rangle_n$ and $\langle H\rangle_{N-n}$ arises when approximate 'magnon states' are chosen. This is for two reasons. Firstly, there are different numbers of unphysical states involved in the chosen magnon basic states n and $(N-n)$ as discussed in appendix A. Secondly, the composite state obtained from the n-magnon state after inverting the z-axis is different from the $(N-n)$-magnon state with the normal z-axis. The linear combination coefficients are different, causing a slight difference in energy.

3. Crystal characteristics

The structural characteristics of a single crystal are briefly reviewed here so that the subsequent theoretical formalism remains valid for all Bravais lattices. In a (three-dimensional) solid, three orthogonal axes can be chosen. The first axis (1) by default has two nearest neighbors ($z_1 = 2$) along one direction (ε_1). The second axis (2) forms a plane, and there can be z_2 nearest neighbors along $z_2/2$ directions $(\varepsilon_2, \ldots, \varepsilon_{1+z2/2})$ with equal coupling constants ($J_2 = \cdots = J_{1+z2/2}$). The third axis (3) can have z_3 nearest neighbors along $z_3/2$ directions $(\varepsilon_{2+z2/2}, \ldots, \varepsilon_{1+z2/2+z3/2})$ with equal coupling constants ($J_{2+z2/2} = \cdots = J_{1+z2/2+z3/2}$). The total number of nearest neighbors is written as $z = z_1 + z_2 + z_3$. A list of nearest-neighbor directions and the coupling constants for 14 Bravais lattices is given in table 3. The vectors connecting nearest neighbors are written as $\boldsymbol{\delta}_\varepsilon$ whereas a_1, a_2 and a_3 denote the lattice constants. The magnon wave vectors along each axis in the reciprocal lattice are to be written as

$$\boldsymbol{k}_i = \frac{m_i}{N_i}\boldsymbol{b}_i, \qquad \text{for } m_i = -\frac{N_i}{2}+1, \ldots, \frac{N_i}{2}, \tag{16}$$

where $\boldsymbol{b}_1$, $\boldsymbol{b}_2$ and $\boldsymbol{b}_3$ are reciprocal lattice vectors. There are a total of N unit cells, and N_1, N_2 and N_3 are the number of cells along the reciprocal axes. Obviously, $N = N_1N_2N_3 = \bar{N}^3$. The scalar product $\boldsymbol{k}_i\cdot\boldsymbol{\delta}_\varepsilon$ gives rise to the familiar $2\pi m_i/N_i a_i$ term because the nearest-neighbor vectors are merely linear combinations of the primitive lattice vectors. The distribution of magnon wave vectors is just like that for a free-electron Fermi gas. This will influence the form of our subsequent results.

For a three-dimensional crystal, the total number of excitations $n = \sum_k n_k$ is written as

$$n = \int \mathrm{d}^3m\, \mathsf{N}(\boldsymbol{m}) \tag{17}$$

where $\mathsf{N}(\boldsymbol{m})$ is defined by $\mathsf{N}(\boldsymbol{m}) = \sum_{i=1}^{n}\delta^3(\boldsymbol{m}-\boldsymbol{m}_i)$. At any specific point $\boldsymbol{m}$ in the reciprocal lattice there can be a maximum of $2S$ magnons. We notice that $\overline{\mathsf{N}(\boldsymbol{m})} = n/N$. The characteristics described here will remain valid for the present work, and also for the subsequent papers.

Table 3. Bravais lattice characteristics that are necessary for the present treatment.

(Number of nearest neighbors) Bravais lattice	(Nearest-neighbor directions) coupling constants	$\sum_\varepsilon J_\varepsilon \cos \boldsymbol{k}\cdot\boldsymbol{\delta}_\varepsilon$
I. ($z=6$)	$(\varepsilon_1,\varepsilon_2,\varepsilon_3)$	
Cubic P	$J_1=J_2=J_3$	$J_1\cos(2\pi m_1/N_1)+J_2\cos(2\pi m_2/N_2)+J_3\cos(2\pi m_3/N_3)$
Tetragonal P	$J_1=J_2\neq J_3$	
Orthorhombic P	$J_1\neq J_2\neq J_3$	
Triclinic P	$J_1\neq J_2\neq J_3$	
Monoclinic P with $\beta\sim 90^\circ$	$J_1\neq J_2\neq J_3$	
Trigonal R with $\alpha=\beta=\gamma\sim 90^\circ$	$J_1=J_2=J_3$	
Orthorhombic C	$J_1=J_2\neq J_3$	
Monoclinic C with $\beta\sim 90^\circ$	$J_1=J_2\neq J_3$	
II. ($z=8$)	$(\varepsilon_1-\varepsilon_4)$	
Cubic I	$J_1=J_2=J_3=J_4$	$J_1[\cos(2\pi m_1/N_1)+\cos(2\pi m_2/N_2)+\cos(2\pi m_3/N_3)$
Tetragonal I	$J_1=J_2=J_3=J_4$	$+\cos 2\pi(-m_1/N_1+m_2/N_2+m_3/N_3)]$
Orthorhombic I	$J_1=J_2=J_3=J_4$	
III. ($z=12$)	$(\varepsilon_1,\varepsilon_2,\varepsilon_3-\varepsilon_6)$	$J_1[\cos(2\pi m_1/N_1)+\cos(2\pi m_2/N_2)]+J_3[\cos(2\pi m_3/N_3)$
Cubic F	$J_1=J_2=J_3=J_4=J_5=J_6$	$+\cos 2\pi(-m_1/N_1-m_2/N_2+m_3/N_3)]+J_5[\cos 2\pi(-m_1/N_1$
Orthorhombic F	$J_1=J_2\neq J_3=J_4\neq J_5=J_6$	$+m_3/N_3)+\cos 2\pi(-m_2/N_2+m_3/N_3)]$
IV. ($z=12$)	$(\varepsilon_1,\varepsilon_2-\varepsilon_3,\varepsilon_4-\varepsilon_6)$	
Hexagonal P	$J_1=J_2=J_3\neq J_4=J_5=J_6$	$J_1[\cos(2\pi m_1/N_1)+\cos 2\pi(m_1/N_1+m_2/N_2)$
Trigonal R with $\alpha=\beta=\gamma\sim 120^\circ$	$J_1=J_2=J_3\neq J_4=J_5=J_6$	$+\cos(2\pi m_2/N_2)]+J_4[\cos(2\pi m_3/N_3)+\cos 2\pi(m_3/N_3$ $-m_1/N_1)+\cos 2\pi(m_3/N_3-m_1/N_1-m_2/N_2)]$

Table 4. The zeroth-order energy expressions $\varepsilon_n^{(0)}$ for the different types of Bravais lattice. Here we take $M_1=J_1^{1/2}m_1/N_1$, $M_2=J_2^{1/2}m_2/N_2$ and $M_3=J_3^{1/2}m_3/N_3$.

Lattice (number of nearest neighbors)	$\varepsilon_n^{(0)}$
Type I ($z=6$)	$4S\sum_k n_k\sum_{p=1}^{\infty}\frac{(-1)^{p+1}(2\pi)^{2p}}{(2p)!}\left[\frac{1}{J_1^{p-1}}M_1^{2p}+\frac{1}{J_2^{p-1}}M_2^{2p}+\frac{1}{J_3^{p-1}}M_3^{2p}\right]$
Type II ($z=8$)	$4S\sum_k n_k\sum_{p=1}^{\infty}\frac{(-1)^{p+1}(2\pi)^{2p}}{(2p)!}\frac{1}{J^{p-1}}[M_1^{2p}+M_2^{2p}+M_3^{2p}+(M_2+M_3-M_1)^{2p}]$
Type III ($z=12$)	$4S\sum_k n_k\sum_{p=1}^{\infty}\frac{(-1)^{p+1}(2\pi)^{2p}}{(2p)!}\otimes\left[J_1\left(\frac{M_1^{2p}}{J_1^p}+\frac{M_2^{2p}}{J_2^p}\right)+J_3\left\{\frac{M_3^{2p}}{J_3^p}+\left(\frac{M_3}{\sqrt{J_3}}-\frac{M_1}{\sqrt{J_1}}-\frac{M_2}{\sqrt{J_2}}\right)^{2p}\right\}\right.$ $\left.+J_5\left\{\left(\frac{M_3}{\sqrt{J_3}}-\frac{M_1}{\sqrt{J_1}}\right)^{2p}+\left(\frac{M_3}{\sqrt{J_3}}-\frac{M_2}{\sqrt{J_2}}\right)^{2p}\right\}\right]$
Type IV ($z=12$)	$4S\sum_k n_k\sum_{p=1}^{\infty}\frac{(-1)^{p+1}(2\pi)^{2p}}{(2p)!}\otimes\left[J_1\left\{\frac{M_1^{2p}}{J_1^p}+\left(\frac{M_1}{\sqrt{J_1}}+\frac{M_2}{\sqrt{J2}}\right)^{2p}+\frac{M_2^{2p}}{J_2^p}\right\}+J_4\left\{\frac{M_3^{2p}}{J_3^p}+\left(\frac{M_3}{\sqrt{J_3}}-\frac{M_1}{\sqrt{J_1}}\right)^{2p}\right.\right.$ $\left.\left.+\left(\frac{M_3}{\sqrt{J_3}}-\frac{M_1}{\sqrt{J_1}}-\frac{M_2}{\sqrt{J_2}}\right)^{2p}\right\}\right]$

4. The zeroth-order treatment

The standard magnon treatment basically relies on the independent magnon picture with ω_k as the zeroth-order one-magnon energy, for an infinite number of independent magnons of each mode. This is normally updated by considering the magnon–magnon interaction. In contrast, the present analysis deals with n-magnon states where n varies from 0 to $2NS$. The zeroth-order energy of each microstate, as given in equation (14), can be written as

$$E_n^{(0)}=-g\mu_B B(NS-n)-zNS^2\bar{J}+\varepsilon_n^{(0)} \tag{18}$$

where

$$\varepsilon_n^{(0)}=4S\int \mathrm{d}^3m\,\mathsf{N}(\boldsymbol{m})\sum_\varepsilon J_\varepsilon\left\{1-\cos\left(\sum_{i=1,2,3}\frac{2\pi m_i\delta_{\varepsilon i}}{N_i\delta_i}\right)\right\} \tag{19}$$

where $\delta_{\varepsilon i}$ are the components of δ_ε along the primitive lattice vectors δ_i's.

We consider an arbitrary brick-like shape such that N_1, N_2 and N_3 can all be different. However, the finally calculated bulk properties need to be shape independent. The average of $\varepsilon_n^{(0)}$ can be correctly written as $\bar{\varepsilon}_n^{(0)}=n\omega_0'$ when the integral in (19) is carried out with variables m_x, m_y and m_z. We make use of the quantities $M_i=J_i^{1/2}m_i/N_i$, $i=1$, 2, 3. This yields analytical expressions for the $\varepsilon_n^{(0)}$ values that are given in table 4, and that satisfy the condition $\varepsilon_n^{(0)}+\varepsilon_{2NS-n}^{(0)}(\text{corresponding})=N\omega_0'$. Therefore,

$$\begin{aligned}\max\varepsilon_{2NS-n}^{(0)}(\text{corresponding})&=N\omega_0'-\min\varepsilon_n^{(0)},\\ \min\varepsilon_{2NS-n}^{(0)}(\text{corresponding})&=N\omega_0'-\max\varepsilon_n^{(0)}.\end{aligned} \tag{20}$$

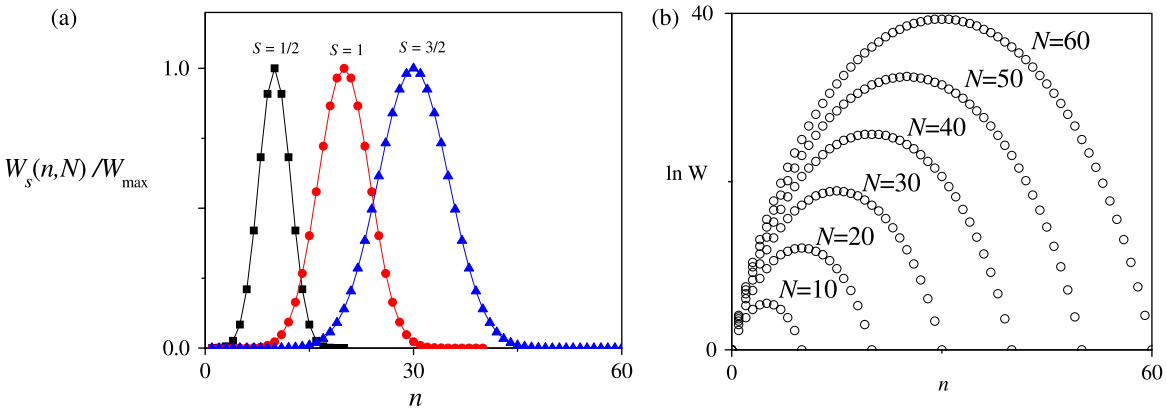

Figure 2. (a) The probability functions $W_S(n, N)$ for $S = 1/2$ ($W_{max} = 1.85 \times 10^5$), 1 ($W_{max} = 3.77 \times 10^8$), and 3/2 ($W_{max} = 8.70 \times 10^{10}$) and $N = 20$. (b) The probability functions ln $W_{1/2}(n, N)$ for $N = 10, 20, 30, 40, 50, 60$.

The minimum value for $\varepsilon_n^{(0)}$ for $n < NS$ can be determined by considering that the m-space is tightly filled around the origin, which implies

$$\int \mathrm{d}^3 m = \frac{4\pi N}{(J_1 J_2 J_3)^{1/2}} \int_0^{M^*} \mathrm{d}M\, M^2 = \frac{n}{2S}. \tag{21}$$

One obtains $M^* = (3n/8\pi SN)^{1/3}(J_1 J_2 J_3)^{1/6}$. The minimum values are given in table 5a for all Bravais lattices. For the maximum values, we consider the corners of the brick shape in the reciprocal lattice to be tightly filled. After some rather detailed calculations, we find the maximum $\varepsilon_n^{(0)}$ values for $J_1 \approx J_2 \approx J_3$. These are shown in table 5b.

At a relatively low temperature, one can resort to the long wavelength limit by considering that the summation over p in table 4 is to be replaced only by the $p = 1$ term. We then find, for a spherically symmetric distribution in m space, the following results:

Type I: (For $J_1/N_1^2 = J_2/N_2^2 = J_3/N_3^2 = \bar{J}/\bar{N}^2$)

$$\omega_0' = 12S\bar{J}; \qquad \bar{J} = (J_1 + J_2 + J_3)/3$$

$$\varepsilon_{n,lt}^{(0)} = \frac{2\pi^2\omega_0'}{3\bar{N}^2} \int \mathrm{d}^3 m\, \mathsf{N}(\boldsymbol{m}) m^2$$

Type II: (For $N_1 = N_2 = N_3 = \bar{N}$)

$$\omega_0' = 16S\bar{J}; \qquad \bar{J} = J_1$$

$$\varepsilon_{n,lt}^{(0)} = \frac{\pi^2\omega_0'}{\bar{N}^2} \int \mathrm{d}^3 m\, \mathsf{N}(\boldsymbol{m}) m^2 \tag{22}$$

Type III: (For $N_1 = N_2 = N_3 = \bar{N}$ and fcc crystal)

$$\omega_0' = 24S\bar{J}; \qquad \bar{J} = J_1$$

$$\varepsilon_{n,lt}^{(0)} = \frac{10\pi^2\omega_0'}{9\bar{N}^2} \int \mathrm{d}^3 m\, \mathsf{N}(\boldsymbol{m}) m^2$$

Type IV: (For $3N_1^2 = 3N_2^2 = N_3^2 = 3^{2/3}\bar{N}^2$)

$$\omega_0' = 24S\bar{J}; \qquad \bar{J} = (J_1 + J_4)/2$$

$$\varepsilon_{n,lt}^{(0)} = \frac{8\pi^2\omega_0'}{3^{5/3}\bar{N}^2} \int \mathrm{d}^3 m\, \mathsf{N}(\boldsymbol{m}) m^2.$$

4.1. Probabilities

The population in each microstate is governed by the ratio $\bar{J}/k_B T$. Only the microstates with the lowest n values have a sizable population in each. Each state with a relatively large n would have a negligibly small magnon population at a finite temperature. Nevertheless, the middle n values have large numbers of microstates, $W_S(n, N)$. The quantity $W_S(n, N)$ is given in appendix B. For $N = 20$, the variation of $W_S(n, N)$ with different S is shown in figure 2(a). Figure 2(b) shows the change of $W_S(n, N)$ for $S = 1/2$ with N values. This number $W_S(n, N)$ leads to a typical grand canonical distribution as discussed in appendix C. Thus the total population in the group of microstates corresponding to the same n is not necessarily negligibly small when n is quite large but less than NS.

It is easy to show that in the long wavelength limit, the minimum and the maximum values of $\varepsilon_n^{(0)}$ for a given n are

$$\varepsilon_{\min}^{(0)} = \bar{\varepsilon}_{n,lt}^{(0)} u^{2/3},$$
$$\varepsilon_{\max}^{(0)} = \bar{\varepsilon}_{n,lt}^{(0)} \frac{[1 - (1-u)^{5/3}]}{u}, \tag{23}$$

where u is the ratio $n/2NS$. The quantity $\bar{\varepsilon}_{n,lt}^{(0)}$ is the average zeroth-order energy in the long wavelength limit, given by

$$\bar{\varepsilon}_{n,lt}^{(0)} = \frac{2\pi^2}{5}\left(\frac{3}{4\pi}\right)^{2/3} \gamma n \omega_0' \tag{24}$$

where $\gamma = 1$ for Type I, 3/2 for Type II, 5/3 for Type III and $4/3^{2/3}$ for Type IV. As $u \to 0$, the minimum and maximum values tend to 0 and $\frac{5}{3}\bar{\varepsilon}_{n,lt}^{(0)}$, respectively. As $u \to 1$, $\varepsilon_{\min}^{(0)} \to \varepsilon_{\max}^{(0)}$. For each microstate corresponding to a given n, $\varepsilon_n^{(0)}$ varies in the range $\varepsilon_{\min}^{(0)} \leqslant \varepsilon_n^{(0)} \leqslant \varepsilon_{\max}^{(0)}$. The energy band diagram for a spin-1/2 system is shown in figure 3.

4.2. Density of states

As there are a large number of microstates for every finite n value, except when $n = 0$ and $n = 2NS$, a description in terms of the density of states will be more suitable. We first define a dimensionless variable y such that $\varepsilon_n^{(0)} = \bar{\varepsilon}_n^{(0)} y$ (or

Table 5a. The zeroth-order minimum energy expressions, Min $\varepsilon_n^{(0)}$, for the different types of Bravais lattice.

Type of Bravais lattice (number of nearest neighbors)	Min $\varepsilon_n^{(0)}$
Type I ($z = 6$)	$12Sn\sum_{p=1}^{\infty}\frac{(-1)^{p+1}(2\pi)^{2p}}{(2p+1)!(2p+3)}\left[\frac{1}{J_1^{p-1}}+\frac{1}{J_2^{p-1}}+\frac{1}{J_3^{p-1}}\right]\left(\frac{3n}{8\pi NS}\right)^{2p/3}(J_1J_2J_3)^{p/3}$
Type II ($z = 8$)	$36SnJ\sum_{p=1}^{\infty}\frac{(-1)^{p+1}(2\pi)^{2p}}{(2p+1)!(2p+3)}\left(\frac{3n}{8\pi NS}\right)^{2p/3}$
Type III ($z = 12$)	$12Sn\sum_{p=1}^{\infty}\frac{(-1)^{p+1}(2\pi)^{2p}}{(2p)!(2p+3)}\left(\frac{3n}{8\pi NS}\right)^{2p/3}(J_1J_2J_3)^{p/3}\otimes\left\{\frac{1}{2p+1}\left[\frac{1}{J_1^{p-1}}+\frac{J_1}{J_2^{p}}+\frac{1}{J_3^{p-1}}\right]+J_5\sum_{r=0}^{2p}(-1)^r\binom{2p}{r}\right.$ $\left.\times\frac{1}{(\sqrt{J_3})^{2p-r}}\frac{1}{(\sqrt{J_1})^{r}}\frac{(r-1)\cdot(r-3)\cdots1}{(2p-r+1)\cdot(2p-r+3)\cdots(2p+1)}\right\}$
Type IV ($z = 12$)	$\sum_{p=1}^{\infty}2S\frac{(-1)^{p+1}(2\pi)^{2p}}{(2p)!}(I_1+I_2)$

Table 5b. The zeroth-order maximum energy expressions, Max $\varepsilon_n^{(0)}$, for the different types of Bravais lattices. These results are valid for $J_1 \approx J_2 \approx J_3$.

Type of Bravais lattice (number of nearest neighbors)	Max $\varepsilon_n^{(0)}$
Type I ($z = 6$)	$2n\omega_0' - 12Sn\sum_{p=1}^{\infty}\frac{(-1)^{p+1}(2\pi)^{2p}}{(2p+1)!(2p+3)}\left[\frac{1}{J_1^{p-1}}+\frac{1}{J_2^{p-1}}+\frac{1}{J_3^{p-1}}\right]\left(\frac{3n}{8\pi NS}\right)^{2p/3}(J_1J_2J_3)^{p/3}$
Type II ($z = 8$)	$2n\omega_0' - 36SnJ\sum_{p=1}^{\infty}\frac{(-1)^{p+1}(2\pi)^{2p}}{(2p+1)!(2p+3)}\left(\frac{3n}{8\pi NS}\right)^{2p/3}$
Type III ($z = 12$)	$2n\omega_0' - 4S\sum_{p=1}^{\infty}2S\frac{(-1)^{p+1}(2\pi)^{2p}}{(2p)!}\otimes\left\{\frac{3n}{2S(2p+3)(2p+1)}\left(\frac{3n}{8\pi NS}\right)^{2p/3}(J_1J_2J_3)^{p/3}\left[\frac{1}{J_1^{p-1}}+\frac{J_1}{J_2^{p}}+\frac{1}{J_3^{p-1}}\right]+2I_3\right\}$
Type IV ($z = 12$)	$2n\omega_0' - 4S\sum_{p=1}^{\infty}2S\frac{(-1)^{p+1}(2\pi)^{2p}}{(2p)!}\otimes\left\{\frac{3n}{2S(2p+3)(2p+1)}\left(\frac{3n}{8\pi NS}\right)^{2p/3}(J_1J_2J_3)^{p/3}\left[\frac{1}{J_1^{p-1}}+\frac{J_1}{J_2^{p}}+\frac{J_4}{J_3^{p}}\right]+I_4+I_5\right\}$

$I_1 = \frac{6n}{(2p+1)(2p+3)}\left(\frac{3n}{8\pi NS}\right)^{2p/3}(J_1J_2J_3)^{p/3}\left\{\frac{1}{J_1^{p-1}}+\frac{J_1}{J_2^{p}}+\frac{J_4}{J_3^{p-1}}\right\}$

$I_2 = \sum_{r=0}^{2p}(-1)^r\binom{2p}{r}\left(\frac{1}{2p+3}\right)\left(\frac{3n}{8\pi NS}\right)^{2p/3}3n(J_1J_2J_3)^{p/3}\left\{\frac{J_1}{(\sqrt{J_1})^{2p-r}}\frac{1}{(\sqrt{J_2})^{r}}\frac{1.3.5\cdots(2p-r-1).1.3.5\cdots(r-3)}{(2p+1)\cdot(2p-1)\cdots1}\oplus\frac{J_4}{(\sqrt{J_3})^{2p-r}}\frac{1}{(\sqrt{J_1})^{r}}\frac{(r-1).(r-3)\cdots1}{(2p-r+1)\cdot(2p-r+3)\cdots(2p+1)}\right\}$

$I_3 = J_5\sum_{r=0}^{2p}\sum_{r'=0}^{r}\binom{2p}{r}\binom{r}{r'}\left(\frac{1}{2}\right)^{2p-r}\frac{1}{(\sqrt{J_1})^{r'}}\frac{1}{(\sqrt{J_3})^{r-r'}}\frac{3n}{8\pi S(r+3)}\left(\frac{3n}{8\pi SN}\right)^{(r-1)/3}(J_1J_2J_3)^{(r-1)/6}\otimes 2\pi\frac{(r'-1)\cdot(r'-3)\cdots1}{(r-r'+1).(r-r'+3)\cdots(r+1)}$

$I_4 = J_1\sum_{r=0}^{2p}\sum_{r'=0}^{r}\binom{2p}{r}\binom{r}{r'}\left(\frac{1}{2}\right)^{2p-r}\frac{1}{(\sqrt{J_1})^{r-r'}}\frac{1}{(\sqrt{J_2})^{r'}}\frac{3n}{8\pi S(r+3)}\left(\frac{3n}{8\pi SN}\right)^{(r-1)/3}(J_1J_2J_3)^{(r-1)/6}\otimes 2\pi\frac{1.3.5\cdots(r-r'+1).1.3\cdots(r-1)}{2^r r!}$

$I_5 = J_4\sum_{r=0}^{2p}\sum_{r'=0}^{r}\binom{2p}{r}\binom{r}{r'}\left(\frac{1}{2}\right)^{2p-r}\frac{1}{(\sqrt{J_1})^{r'}}\frac{1}{(\sqrt{J_3})^{r-r'}}\frac{3n}{8\pi S(r+3)}\left(\frac{3n}{8\pi SN}\right)^{(r-1)/3}(J_1J_2J_3)^{(r-1)/6}\otimes 2\pi\frac{(r'-1)\cdot(r'-3)\cdots1}{(r-r'+1)\cdot(r-r'+3)\cdots(r+1)}$

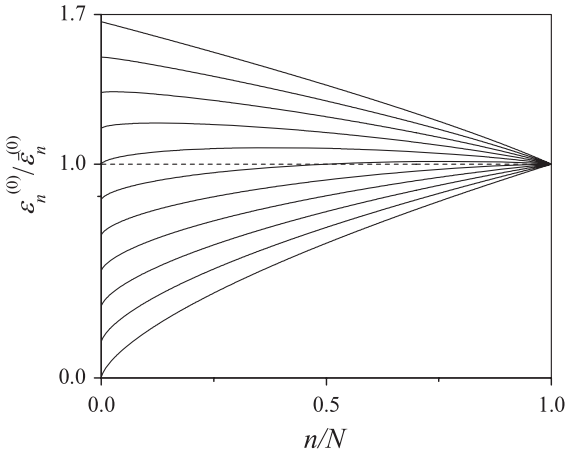

Figure 3. Magnon energy ratio versus number fraction plot for a crystal of spin-1/2 atoms using equation (25). We have used $B = 0$. Solid lines indicate the zeroth-order magnon energy spread in the range $\varepsilon_{\min}^{(0)}(n) \leqslant \varepsilon_n^{(0)} \leqslant \varepsilon_{\max}^{(0)}(n)$.

$\varepsilon_{n,lt}^{(0)} = \bar{\varepsilon}_{n,lt}^{(0)} y$). In the long wavelength approximation, y lies in the range $u^{2/3} \leqslant y \leqslant [1-(1-u)^{5/3}]/u$. The zeroth-order density of states $\rho(\varepsilon_n^{(0)}) = \mathrm{d}N(\varepsilon_n^{(0)})/\mathrm{d}\varepsilon_n^{(0)}$ can be written as $\rho(\varepsilon_n^{(0)}) = g(y)/\bar{\varepsilon}_{n,lt}^{(0)}$, where $g(y) = \mathrm{d}N(y)/\mathrm{d}y$, $\mathrm{d}N(y)$ being the number of states between y and $y + \mathrm{d}y$. For a specific n (not equal to 0 or $2NS$), we get

$$W_S(n,N)^{-1}\int_{y_{\min}}^{y_{\max}}\mathrm{d}y\, g(y) = 1,$$
$$\bar{y} = W_S(n,N)^{-1}\int_{y_{\min}}^{y_{\max}}\mathrm{d}y\, yg(y) = 1. \tag{25}$$

4.3. General spin systems

Considering that $\varepsilon_{1,lt}^{(0)}/\omega_0'$ is proportional to m^2 and also to y, we write

$$g_n(y) = \sum_{n_1,n_2,\ldots,n_N}\frac{\mathcal{J}(y;n_1,n_2,\ldots,n_N)}{\int_{y_{\min}}^{y_{\max}}\mathrm{d}y\,\mathcal{J}(y;n_1,n_2,\ldots,n_N)}\delta_{n,\sum_i n_i} \tag{26}$$

where the function $\mathcal{J}(y; n_1, n_2, \ldots, n_N)$ is given by

$$\begin{aligned}\mathcal{J}(y; n_1, n_2, \ldots, n_N) &= \int_0^{5/3} \mathrm{d}y_1' \, y_1'^{1/2} \\ &\times \int_0^{5/3} \mathrm{d}y_1'' \, y_1''^{1/2} \cdots (n_1 \text{ times}) \otimes \cdots \\ &\otimes \int_0^{5/3} \mathrm{d}y_N' \, y_N'^{1/2} \int_0^{5/3} \mathrm{d}y_N'' \, y_N''^{1/2} \cdots (n_N \text{ times}) \\ &\otimes \prod_{i<j} [1 - \delta(y_i' - y_j')][1 - \delta(y_i' - y_j'')] \cdots \\ &\times [1 - \delta(y_i'' - y_j')][1 - \delta(y_i'' - y_j'')] \cdots \\ &\otimes \delta_{ny}, ([y_1' + y_1'' + \cdots] + [y_2' + y_2'' + \cdots] + \cdots \\ &+ [y_N' + y_N'' \cdots]). \end{aligned} \tag{27}$$

It is easy to verify that $g_n(y)$ in (26) satisfies the general conditions (25). To calculate the denominator in (26), one can replace the product containing the Dirac delta functions by unity and simultaneously change the lower and upper boundaries of y from $y_{\min}$ and $y_{\max}$ to 0 and 5/3. The same maneuver must be applied while calculating the integral over the numerator, $\mathcal{J}(y; n_1, \ldots, n_N)\mathcal{F}(y)$, where $\mathcal{F}(y)$ is any arbitrary function. If we adopt this procedure, the general density of states can be given the simple expression

$$\begin{aligned} g_n(y) &= (\tfrac{3}{2})^n (\tfrac{3}{5})^{3n/2} \\ &\times \sum_{n_1, n_2, \ldots, n_N} \mathcal{J}(y; n_1, n_2, \ldots, n_N) \delta_{n, \sum_i n_i}. \end{aligned} \tag{28}$$

4.4. Thermal population distribution

In traditional magnon formalisms one normally deals with the dispersion laws for the single-particle states. As the magnon operators are like Bose operators, the Planck distribution is invariably adopted in these treatments. The Planck distribution for magnons amounts to including contributions from unphysical states. To avoid this difficulty, we find the distribution function for the physically acceptable states corresponding to each permissible n. This is discussed below.

Considering the zeroth-order energy in equation (22), the unnormalized thermal distribution function for all microstates of n magnons is written from the grand canonical distribution (see appendix C):

$$\begin{aligned} &\phi^{(0)}(0) = 1, \\ &\phi^{(0)}(n) = \mathrm{e}^{-(\mu n + g\mu_{\mathrm{B}} B n)/\tau} \int_{y_{\min}(n)}^{y_{\max}(n)} \mathrm{d}y \, g_n(y) \mathrm{e}^{-\bar{\varepsilon}^{(0)}_{n,lt} y/2S\tau}, \\ &\quad \text{for } 0 < n < 2NS \\ &\phi^{(0)}(2NS) = \mathrm{e}^{-(2NS\mu + 2g\mu_{\mathrm{B}} NSB + \bar{\varepsilon}^{(0)}_{2NS,lt}/2S)/\tau}, \end{aligned} \tag{29}$$

where μ is the chemical potential, $\tau = k_{\mathrm{B}}T$, k_{B} being the Boltzmann constant and T the temperature in kelvin. Here we have used the standard expression $\beta = 1/\tau$ as the number of states is exceedingly large. If one inserts expression (28) for the density of states in (29), removes the delta function containing terms and accordingly adjusts the boundaries of y, one obtains

$$\phi^{(0)}(n) = W_S(n, N) \left(\frac{\phi^{(0)}(1)}{N} \right)^n \tag{30}$$

where the distribution function for the one-magnon states is given by

$$\phi^{(0)}(1) = \tfrac{3}{2}(\tfrac{3}{5})^{3/2} N \mathrm{e}^{-(\mu + g\mu_{\mathrm{B}} B)/\tau} \int_0^{5/3} \mathrm{d}y \, \sqrt{y} \mathrm{e}^{-\bar{\varepsilon}^{(0)}_{1,lt} y/2S\tau}. \tag{31}$$

The sum of unnormalized distribution functions over all possible numbers of magnons is now calculated. In appendix D, it is shown that although for a general spin S the explicit functional form of $W_S(n, N)$ is difficult to calculate (except when $S = 1/2$), the sum in the denominator has a simple appearance because of the properties of $W_S(n, N)$. Using (D.4), we get the normalized magnon distribution

$$\Phi^{(0)}(n) = \frac{\phi^{(0)}(n)}{\sum_{n=0}^{2NS} \phi^{(0)}(n)} = W_S(n, N) x^{(0)^n} \left(\frac{1 - x^{(0)}}{1 - x^{(0)^{2S+1}}} \right)^N \tag{32}$$

where $x^{(0)} = \phi^{(0)}(1)/N$.

5. Physical properties

5.1. Magnon number

We now calculate the zeroth-order thermal average of the total number of magnons,

$$\langle n \rangle_T^{(0)} = \sum_{n=0}^{2NS} n \Phi^{(0)}(n). \tag{33}$$

Using (D.5) from appendix D, we get

$$\langle n \rangle_T^{(0)} = NS[1 - B_S(\theta)] \tag{34}$$

where $\theta = -S \ln x^{(0)}$ and $B_S(\theta)$ is the Brillouin function. Henceforth we will consider the chemical potential as $\mu = 0$. As $\tau/\bar{J} \to \infty$, $\langle n \rangle_T \to NS$ that shows all magnon states to be equally populated. As $\tau/\bar{J} \to 0$,

$$\langle n \rangle_T^{(0)} \to \frac{3}{2} \left(\frac{3}{5} \right)^{3/2} N \left(\frac{\tau}{\bar{\varepsilon}^{(0)}_{1,lt}} \right)^{3/2} \Gamma(3/2) \mathrm{e}^{-g\mu_{\mathrm{B}} B/\tau}. \tag{35}$$

One may consider the mean field approximation and adopt the molecular (Weiss) field [11] $B_{\mathrm{mol}} = \lambda^{(0)} M$ such that $B = B_{\mathrm{app}} + B_{\mathrm{mol}}$ where B_{app} is the applied magnetic field. Here we note two important deviations from the standard formulation, namely the absence of the Riemannian zeta function and the introduction of the molecular field. The zeta function arises from the mixing of the unphysical states that is inherent in the infinite sums involved firstly in Planck distribution and secondly in the infinite sum instead of the finite sum in (33). Both $\lambda^{(0)}$ and M are dependent on temperature.

5.2. Molecular field constant

The so-called molecular field constant λ arises from the additional stabilization caused by spin flips. The excess stability can be understood from resonating valence bond theory [9b, 9c, 9d, 9e]. It can also be interpreted as the increase in the number of lines of force at the 'up' spin sites

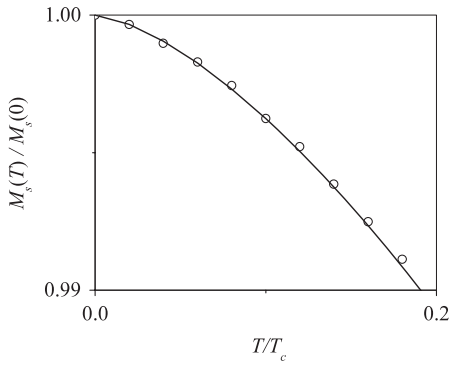

Figure 4. $M_s^{(0)}(T)/M_s^{(0)}(0)$ versus T/T_c graph. The solid line represents the theoretically calculated curve and dots are for experimental data points for Ni crystal from [12].

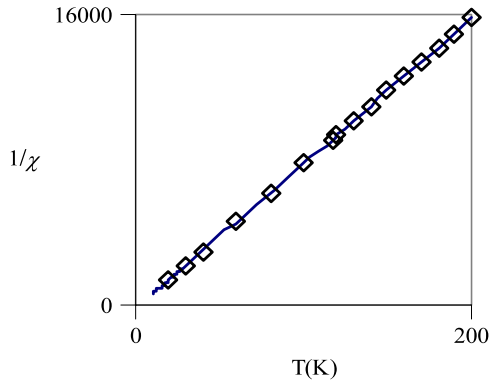

Figure 5. Variation of $1/\chi$ with T for ammonium vanadium (III) fluorophosphates. The solid line is the theoretically determined curve and dots represent the experimental data points.

due to a 'down' spin nearby, and vice versa. As the number of spin flips changes with temperature, λ also changes. At an extremely low temperature, there would be only a few spin flips that are distributed away from each other. Hence λ becomes linearly proportional to internal energy per spin flip, that is, proportional to T. This is indeed found from the present treatment. As $\tau/\bar{J} \to 0$, we observe from (34)

$$\lambda^{(0)} = \frac{\tau}{n_B g^2 \mu_B^2 (NS - \langle n \rangle_T)} \left[-0.4816 + \frac{3}{2} \ln \frac{2S\tau}{\bar{\varepsilon}_{1,lt}^{(0)}} - \ln \frac{\langle n \rangle_T}{N} \right] - \frac{B_{\text{app}}}{M}. \tag{36}$$

A careful analysis shows that $\lambda^{(0)}$ initially becomes more or less proportional to T. As T increases towards T_c, $\lambda^{(0)}$ increases more slowly with T. The values of $\lambda^{(0)}$ that have been calculated from experimental ΔM_S for nickel at low temperature are given in [12]. Beyond $T/T_c = 0.2$, equation (36) is no longer valid.

5.3. Magnetization

The magnetization is written as $M_S = n_B g \mu_B (NS - \langle n \rangle_T)$ where n_B is the effective magnon number/f.u. Henceforth, without the loss of any generality, we will take N as the total number of spin centers per unit volume. As $\tau/\bar{J} \to \infty$, $M_S \to 0$. The saturation magnetization is given by $M_S(0) = n_B g \mu_B NS$. The magnetization reversal at low temperature ($\tau/\bar{J} \ll 1$), $\Delta M_S = M_S(0) - M_S(T) = n_B g \mu_B \langle n \rangle_T$, is found as

$$\Delta M_S = 0.6178 n_{uc} n_B \left(\frac{g\mu_B}{v_{uc}} \right) \left(\frac{\tau}{\bar{\varepsilon}_{1,lt}^{(0)}} \right)^{3/2} e^{-g\mu_B B/\tau} \tag{37}$$

where n_{uc} is the number of spin centers per unit volume and v_{uc} is the unit cell volume. In equation (37), ΔM_S is $(\frac{g\mu_B}{v_{uc}})(\frac{\tau}{2SJ})^{3/2}$ times a multiplicative factor. The latter replaces the factor 0.117 in [6], but this holds only for Type I solids. In in [6] the factor 0.117 contains additionally the zeta function $\zeta(3/2, 1) = 2.606$ and the author makes an implicit use of $S = 1/2, z = 6$, (corresponding $\gamma = 1$) and $n_{uc} n_B = 1$, and omits the exponential function.

Nickel is a fcc crystal ($N = 9.140 \times 10^{22}$). A statistical mechanical treatment using the moment expansion method gives $\bar{J} = 2.54 k_B T_c/z$ for $S = 1/2$ and $z = 12$ [13]. We get $\bar{J} = 11.51$ meV for $T_c = 631$ K. The $\bar{J}$ so determined is actually related to the zeroth-order energy of Type I systems through equation (24). Hence, for Type III crystals we write $\bar{J}_{\text{mod}} = \bar{J}/\gamma$.

One observes that for $0 \leqslant T/T_c \leqslant 0.2$, $\lambda^{(0)}$ is indeed given by $\lambda^{(0)} = 2900 T/T_c$ for nickel. Using this result, we compute $M_S(T)/M_S(0)$ using equation (37). The calculated plot of $M_S(T)/M_S(0)$ versus T/T_c for nickel ($S = 1/2$) is compared with the experimental data points [12] in figure 4, for $B = 0$.

5.4. Susceptibility

The susceptibility is defined by $\chi = (\mathrm{d}M/\mathrm{d}B_{\text{app}})_{B_{\text{app}}=0}$. The zeroth-order value is found as

$$\chi^{(0)}(T) = \frac{C^{(0)}(T)}{T - \theta^{(0)}(T)} \tag{38}$$

where

$$\begin{aligned} C^{(0)}(T) &= N \frac{n_B g^2 \mu_B^2}{k_B} \xi(T) x_0^{(0)}, \\ x_0^{(0)} &= x^{(0)}|_{B_{\text{app}}=0}, \\ \xi(T) &= \left\{ \frac{1}{(1 - x_0^{(0)})^2} - \frac{(2S+1)^2 x_0^{0^{2S}}}{(1 - x_0^{(0)^{2S+1}})^2} \right\}, \\ \theta^{(0)}(T) &= \lambda^{(0)}(T) C^{(0)}(T). \end{aligned} \tag{39}$$

At a very high temperature ($\tau \gg z\bar{J}$), $x_0^{(0)} \approx 1$ so that $C^{(0)}(T) \approx C^{(0)}(\infty) = N n_B g^2 \mu_B^2 S(S+1)/3k_B$, and $\theta^{(0)}(T) \approx \theta_c^{(0)} = \lambda^{(0)}(\infty) C^{(0)}(\infty)$. This yields the Curie–Weiss law in zeroth order, $\chi^{(0)}(T) = C^{(0)}(\infty)/(T - \theta_c^{(0)})$.

Ammonium vanadate (III) fluorophosphate ($S = 1$) forms an orthorhombic crystal with $T_c = 2.7$ K [14] and density 2.62 g cc^{-1}. The molecular mass is 182.9, so that $N = 8.56 \times 10^{21}$. Using $n_B = 1$, we get $C^{(0)}(\infty) = 35.02 \times 10^{-2} g^2$ and $\lambda^{(0)}(\infty) = 770.8 g^{-2}$. Figure 5 shows the variation of $1/\chi$ with temperature. The agreement with the experimental

results is achieved for $g = 1.886$, which is close to the estimate 1.85 [14].

At a very low temperature ($\tau/z\bar{J} \to 0$), $x_0^{(0)} \to 0$. Therefore $\xi(T) \to 1$, $C^{(0)}(T) \to 0$, $\theta^{(0)}(T) \to 0$, and $\chi^{(0)} \to C^{(0)}(T)/T$. It can be shown that

$$\chi^{(0)}(T) = \frac{3}{2}\left(\frac{3}{5}\right)^{3/2}\Gamma(3/2)n_B N g^2\mu_B^2\frac{\tau^{1/2}}{\bar{\varepsilon}_{1,lt}^{(0)3/2}}e^{-g\mu_B B/\tau}. \quad (40)$$

At temperatures in the middle range, $\chi^{(0)}(T)$ can be generally expanded into the power series

$$\chi^{(0)}(T) = \frac{C^{(0)}(\infty)}{T}\sum_{l=0}^{\infty} a_l(T_c/T)^l \quad (41)$$

where $a_0 = 1$. This formula was first derived by Domb and Sykes [15a] and Rushbrooke and Wood [15b]. Furthermore, following Padé approximant analysis by Gammel *et al* [16], $1/\chi(T)$ is seen to diverge as $(T - T_c)^{4/3}$ for cubic lattices near the Curie point. Kouvel and Fischer also made a detailed investigation of the magnetic behavior of nickel near its Curie point and found $\chi^{(0)-1} = A[T - T_c]^{\gamma}$ with $\gamma = 1.35 \pm 0.02$ [17]. However, the integral in $x_0^{(0)}$ is much less than $(2/3)(5/3)^{3/2}$ near $T = T_c$, and the argument of the Brillouin function largely differs from $\mu_B(B_{app} + \lambda M)/\tau$.

One question that arises is why this behavior of χ emerges from the zeroth-order treatment. The answer is that at a temperature around the Curie point or lower, only a few magnons are created as $\varepsilon_1^{(0)}$ is of the order of $k_B T_c$. The interaction is negligibly feeble (the weak coupling limit), and the magnetic behavior can be predicted from the zeroth-order treatment.

5.5. Heat capacity

The zeroth-order internal energy $U^{(0)}$ is given by

$$U^{(0)} = \left\{\sum_{n=1}^{2NS-1} e^{-(\mu n + g\mu_B Bn)/\tau} \times \int_{y_{min}(n)}^{y_{max}(n)} dy\,(\bar{\varepsilon}_n^{(0)}y)g_n(y)e^{-\bar{\varepsilon}_{n,lt}^{(0)}y/\tau} + \bar{\varepsilon}_{2NS}^{(0)} \times e^{-(2NS\mu + 2g\mu_B NSB + \bar{\varepsilon}_{2NS,lt}^{(0)})/\tau}\right\} \Big/ \sum_{n=0}^{2NS} W_n(n, N)x^{(0)n}. \quad (42)$$

For $\mu = 0$, and as $N \to \infty$, we find

$$U^{(0)} = \frac{3}{2}\left(\frac{3}{5}\right)^{3/2}\bar{\varepsilon}_{1,lt}^{(0)}\frac{1}{x^{(0)}}\frac{S_2(x^{(0)}, N)}{S_1(x^{(0)}, N)}e^{-g\mu_B(B_{app}+\lambda^{(0)}M)/\tau} \times \int_0^{5/3} dy\, y^{3/2}e^{-\bar{\varepsilon}_{1,lt}^{(0)}y/\tau} \quad (43)$$

where $S_1(x^{(0)}, N)$ and $S_2(x^{(0)}, N)$ are the standard sums as given in appendix D. This implies

$$U^{(0)} = \langle n\rangle_T^{(0)}\bar{\varepsilon}_{1,lt}^{(0)}\frac{\int_0^{5/3} dy\, y^{3/2}e^{-\bar{\varepsilon}_{1,lt}^{(0)}y/\tau}}{\int_0^{5/3} dy\, y^{1/2}e^{-\bar{\varepsilon}_{1,lt}^{(0)}y/\tau}}. \quad (44)$$

In the low temperature limit ($\tau/\bar{J} \to 0$), the internal energy is proportional to $T^{5/2}$ as in the traditional treatment, but it is also proportional to an exponential term:

$$U^{(0)} = \frac{3}{2}\left(\frac{3}{5}\right)^{3/2}\Gamma(5/2)N\bar{\varepsilon}_{1,lt}^{(0)}\left(\frac{\tau}{\bar{\varepsilon}_{1,lt}^{(0)}}\right)^{5/2}e^{-g\mu_B(B_{app}+\lambda^{(0)}M)/\tau}. \quad (45)$$

The ratio $g\mu_B\gamma^{(0)}M/\tau$ is of the order of unity (1.36 at $T/T_c = 0.1$ for nickel). The corresponding heat capacity (C_v) is

$$C_v^{(0)} = \frac{15}{4}\left(\frac{3}{5}\right)^{3/2}\Gamma(5/2)Nk_B\left(\frac{\tau}{\bar{\varepsilon}_{1,lt}^{(0)}}\right)^{3/2} \times \left[1 + \frac{2g\mu_B(B_{app} + \lambda^{(0)}M)}{5\tau}\right]e^{-g\mu_B(B_{app}+\lambda^{(0)}M)/\tau} \quad (46)$$

in approximate agreement with Bloch's $T^{3/2}$ law [18]. The agreement improves when $(B_{app} + g\mu_B\gamma^{(0)}M/\tau) \to 0$. The variation of $U^{(0)}$ and $C_v^{(0)}$ with temperature is given in figures 6(a) and (b) for $(NH_4)[VPO_4F]$ and nickel crystals.

In the high temperature limit ($\tau/\bar{J} \to \infty$) we find $U^{(0)} = N\bar{\varepsilon}_{1,lt}^{(0)}$ and subsequently $C_v^{(0)} = 0$. This may be rationalized using the example of a transition metal complex where $\bar{J}$ is quite small as the metal centers are far apart from each other. With the rise of temperature, all local (site) states become almost equally populated, resulting in a net zero heat capacity. Similarly in our formalism, all the $(2S + 1)^N$ magnon states tend to become equally populated as $T \to \infty$. The traditional treatment, however, deals with an infinite number of states which are mostly unphysical, and the high temperature limit gives $C_v^{(0)} \propto Nk_B$. The present formalism obviously shows a physically acceptable result.

5.6. Discussion

From observed data, we find the temperature dependence of λ and $\langle n\rangle_T$ as shown in figure 7. The low temperature ($T < T_c$) values for $\langle n\rangle_T$ and $\lambda^{(0)}$ have been obtained from ΔM_S data [12] and using equation (37). At low temperatures, $\lambda^{(0)}$ almost equals λ. The higher temperature values have been retrieved from the χ values [19] for nickel at $T > T_c$ and the generalized Curie–Weiss law $\chi = C(T)/(T - \lambda(T)C(T))$. We have approximated λ as $\lambda = T\,d(1/\chi)/dT - 1/\chi$, which holds at higher temperatures where C and λ become nearly independent of temperature. The $\langle n\rangle_T$ values have been calculated from $\langle n\rangle_T = \Delta M_S(T)/n_B g\mu_B$ for a magnetic field of 12 kG. The effective magnon number n_B equals 0.606 for nickel ($S = 1/2$ system).

Figure 7 also shows $\langle n\rangle_T$ as a function of temperature. It is obvious that $\langle n\rangle_T$ exhibits a big jump just after T_c. The reason is that, as the Rushbrooke and Wood [15b] formula implies, $k_B T_c$ is the critical energy required for a spin flip. In consequence, λ also exhibits a jump right after T_c, and then it slowly increases to a saturation value (λ_∞).

The quantity $\langle n\rangle_T^{(0)}$ has been calculated from equation (34) for $T > T_c$, using the estimated λ values. Figure 7 reveals that with a finite number of states the calculated $\langle n\rangle_T^{(0)}$ differs greatly from the observed $\langle n\rangle_T$.

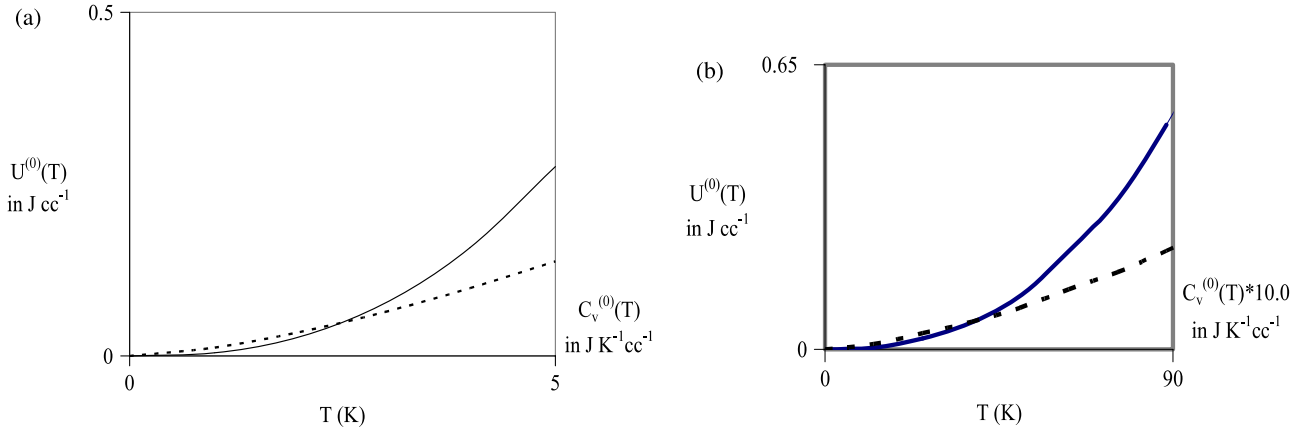

Figure 6. (a) The variation of zeroth-order internal energy (solid line) and heat capacity (dotted line) with temperature for ammonium vanadium (III) fluorophosphates in zero field. We retained the same molecular specifications as discussed in [14] and assumed $g\mu_B\gamma^{(0)}M/\tau \approx 0$. (b) Variation of zeroth-order internal energy (solid line) and heat capacity (dotted line) with temperature for nickel. We have taken $B_{app} = 12$ kG and the corresponding M values from experimental data given in [6]. The quantity $\gamma^{(0)}$ has been calculated from a self-consistent procedure.

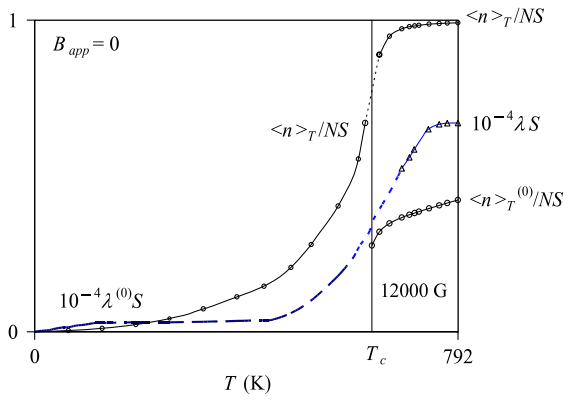

Figure 7. Variation with temperature of $\lambda^{(0)}$ (△) and magnon population $\langle n\rangle_T$ (○) for nickel. Both quantities have been calculated from experimental data. The low temperature values for $\langle n\rangle_T$ and $\lambda^{(0)}$ have been obtained from ΔM_S data and using equation (37). The high temperature values have been retrieved from measured susceptibility.

6. Conclusions

We have recast the spin Hamiltonian in a form to take account of the whole effect of Holstein–Primakoff transformations. We consider only physically acceptable states which are finite in number. The density of n-magnon states where n varies from 0 to $2NS$ has been found. The zeroth-order treatment has been carried out using appropriate mathematical tools derived here for a general S value.

One major outcome is the finding that the so-called molecular field constant λ is dependent on temperature. It increases from zero value (at absolute zero) as the temperature increases, and at a very high temperature attains a saturation value. This behavior is related to the increasing number of spin flips with temperature. When $T < T_c$, the zeroth-order treatment gives reasonably good results. For $T > T_c$, some of the physical properties calculated at the zeroth order would be quite bad.

We show in paper II [7] that at low temperatures, the first-order correction to λ is exceedingly small and the correction to $\langle n\rangle_T$ involves $T^{5/2}$ and $T^{7/2}$ temperature dependences. Around T_c, a T^4 dependent term becomes relevant, as pointed out by Dyson [10]. The quantity $\langle n\rangle_T$ corrected through first order is close to the experimental $\langle n\rangle_T$ in the higher temperature region.

Acknowledgments

Financial support from CSIR is gratefully acknowledged. AP thanks CSIR for a fellowship. The authors are indebted to G Mukhopadhyay for various discussions.

Appendix A. Magnon states

Let us consider a crystal of spin-1/2 sites, limiting the number of site excitations to 0 and 1. There can be n down spins and $(N - n)$ up spins (n site excitations) or vice versa ($N - n$ excitations). The chosen states in the site mode are as follows:

$$\prod_{s=1}^{n}|1_S\rangle = N^{-n/2}\left(\prod_{s=1}^{n}\sum_{k=1}^{N}e^{ik\cdot s}b_k^\dagger\right)|0\rangle \qquad (A.1)$$

and

$$\prod_{s=n+1}^{N}|1_S\rangle = N^{-(N-n)/2}\left(\prod_{s=n+1}^{n}\sum_{k=1}^{N}e^{ik\cdot s}b_k^\dagger\right)|0\rangle. \qquad (A.2)$$

The $\binom{N}{2}$ number of two-site states of type $|1_{j_1}1_{j_2}\rangle = a_{j_1}^\dagger a_{j_2}^\dagger|0\rangle$ form an orthonormal complete set. The two-magnon basis can be chosen as

$$|1_k1_l\rangle = b_k^\dagger b_l^\dagger|0\rangle = N^{-1}\sum_{j_1\neq j_2}e^{-i(k\cdot j_1+l\cdot j_2)}a_{j_1}^\dagger a_{j_2}^\dagger|0\rangle + N^{-1}\sum_j e^{-i(k+l)\cdot j}a_j^{\dagger 2}|0\rangle \qquad (A.3)$$

where $\boldsymbol{k}$ and $\boldsymbol{l}$ are enumerated such that $\boldsymbol{k} < \boldsymbol{l}$. The last term in equation (A.3) contributes unphysical states. This contribution can be removed and the remaining part can be renormalized to write

$$\widetilde{|1_k 1_l\rangle} = \frac{1}{N}\left(1 - \frac{2}{N}\right)^{-1/2} \sum_{j_1 \neq j_2} \mathrm{e}^{-\mathrm{i}(k\cdot j_1 + l\cdot j_2)} a^\dagger_{j_1} a^\dagger_{j_2} |0\rangle. \quad \text{(A.4)}$$

It can be easily shown that with the choice $\boldsymbol{k} < \boldsymbol{l}$, the states $\widetilde{|1_k 1_l\rangle}$ form an orthonormal complete set in the two-magnon sector. Similarly, the three-magnon bases may be chosen as

$$\widetilde{|1_k 1_l 1_m\rangle} = \frac{1}{(N^3 - 6N^2 + 12N)^{1/2}} \times \sum_{j_1 \neq j_2 \neq j_3} \mathrm{e}^{-\mathrm{i}(k\cdot j_1 + l\cdot j_2 + m\cdot j_3)} a^\dagger_{j_1} a^\dagger_{j_2} a^\dagger_{j_3} |0\rangle. \quad \text{(A.5)}$$

For $S = 1$, the two-magnon states can be chosen as either $|1_k 1_l\rangle$ for $\boldsymbol{k} < \boldsymbol{l}$, or as $|2_k\rangle$. The three-magnon bases can be written as

$$\widetilde{|1_k 1_l 1_m\rangle} \frac{N}{(N^2 - 3N + 9N)^{1/2}} \times \left\{ |1_k 1_l 1_m\rangle - N^{-3/2} \sum_j \mathrm{e}^{-\mathrm{i}(k+l+m)\cdot j} a^{\dagger 3}_j |0\rangle \right\}. \quad \text{(A.6)}$$

For other spins, the site states are of the form

$$|n_{j_1} n_{j_2} \cdots\rangle = N^{-n/2} \prod_{j=1}^{N} \left(\sum_{k=1}^{N} \mathrm{e}^{\mathrm{i}k\cdot s} b^\dagger_k \right)^{n_j} |0\rangle \quad \text{(A.7)}$$

with $0 \leqslant n_j \leqslant 2S$, so that the magnon product states of type $|n_{k_1} n_{k_2} \cdots\rangle$ with $0 \leqslant n_k \leqslant 2S$ and $\sum_{k=1}^{N} n_k = n$ can form a basis set in the n-magnon sector. It would be possible to discard the unphysical parts and obtain the renormalized basic states of type $\widetilde{|n_{k_1} n_{k_2} \cdots\rangle}$.

We further notice that because of the unphysical states, the bases $|n_{k_1} n_{k_2} \cdots\rangle$ are in error of order (n/N), and the average values calculated with these would deviate at order $(n/N)^2$.

A.1. Symmetry aspects

The state $\widetilde{|1_k 1_l\rangle}$ is constructed considering the positive z-axis as the direction of the external magnetic field. In the absence of any external magnetic field, inversion of the z-axis through 180° transforms $\widetilde{|1_k 1_l\rangle}$ into the $(N-2)$ composite magnon state $\widetilde{|0_k 0_l\rangle}$ which can be written as

$$\widetilde{|0_k 0_l\rangle} = \frac{1}{\sqrt{N(N-2)}} \sum_{j_1 \neq j_2} \mathrm{e}^{-\mathrm{i}(k\cdot j_1 + l\cdot j_2)} |1_{j'} 1_{j''} \cdots 0_{j_1} 0_{j_2} \cdots\rangle. \quad \text{(A.8)}$$

We consider $\boldsymbol{K} = \boldsymbol{k} + \boldsymbol{l}$, and an inversion of the z-axis converts $\boldsymbol{k}, \boldsymbol{l}$ and $\boldsymbol{K}$ into $\tilde{\boldsymbol{k}}$, $\tilde{\boldsymbol{l}}$ and $\tilde{\boldsymbol{K}}$. The $(N-2)$ magnon state that is complementary to $\widetilde{|1_k 1_l\rangle}$ is written as

$$|1_{k_1} \widetilde{1_{k_2} \cdots 0_k} 0_l \cdots\rangle = \mathcal{N} \sum_{\substack{j' \neq j'' \neq j''' \neq \cdots \\ (\neq j_1, \neq j_2 \cdots)}} \mathrm{e}^{-\mathrm{i}(k_1\cdot j' + k_2 \cdot j'' + k_3 \cdot j''' + \cdots)} |1'_j 1''_j \cdots 0_{j_1} 0_{j_2} \cdots\rangle \quad \text{(A.9)}$$

where $\mathcal{N}$ is the corresponding normalization constant. The Fourier coefficients in (A.8) and (A.9) are obviously different.

Appendix B. Number of microstates

In view of appendix A for the choice of the magnon states, where each magnon mode can have a maximum of $2S$ magnons, the number of microstates with n magnons is given by

$$W_S(n, N) = \sum_{N_0, N_1, \ldots, N_{2S}} \frac{N!}{N_0! N_1! \cdots N_{2S}!} \quad \text{(B.1)}$$

subject to the conditions

$$\sum_{p=0}^{2S} N_p = N, \quad \text{(B.2)}$$

$$\sum_{p=0}^{\min(n, 2S)} p N_p = n. \quad \text{(B.3)}$$

In the above, N_p is the number of modes each of which is occupied by p magnons.

Based on the definition (B.1), the properties of W_S functions are as follows.

(i) *Symmetry*:

$$W_S(n, N) = W_S(2NS - n, N). \quad \text{(B.4)}$$

(ii) *Boundary values*:

$$W_S(0, N) = 1;$$

$$W_S(1, N) = N;$$

$$W_S(2, N) = \begin{cases} N(N-1)/2 & \text{for } S = 1/2, \\ N(N+1)/2 & \text{for } S = 1, 3/2, \ldots; \end{cases} \quad \text{(B.5)}$$

$$W_S(3, N) \sim N^3/3!, \qquad \text{etc.}$$

These are obvious from (B.1).

(iii) *Sum rule*:

$$\sum_{n=0}^{2NS} W_S(n, N) = (2S+1)^N. \quad \text{(B.6)}$$

The proof of this relation relies on the fact that summation over n removes the restriction (B.3) from the sum, and on the multinomial theorem.

(iv) *Regression*:

$$W_S(n, N) = \sum_{p=0}^{\min(n, 2S)} W_S(n - p, N - 1). \quad \text{(B.7)}$$

To show that the regression is consistent with the sum rule, one can write

$$\sum_{n=0}^{2S(N-1)} W_S(n, N) = (2S+1) \sum_{p=0}^{2S(N-1)} W_S(n, N-1) - \sum_{p=1}^{2S} p W_S(2S(N-2) + p, N-1)$$

and

$$\sum_{n=2S(N-1)+1}^{2NS} W_S(n, N) = \sum_{p=1}^{2S} p W_S(2S(N-2) + p, N-1)$$

so that

$$\sum_{n=0}^{2NS} W_S(n, N) = (2S+1) \sum_{n=0}^{2S(N-1)} W_S(n, N-1).$$

On iteration, one retrieves the sum rule (B.6).

(v) *Average*

$$\frac{n}{N} = \sum_{p=1}^{\min(n,2S)} \frac{pW_S(n-p, N-1)}{W_S(n, N)}. \tag{B.8}$$

The proof is based on expanding $pW_S(n-p, N-1)$ and using (B.3).

Appendix C. Thermal distribution

We write (B.1) in a slightly different form

$$W_S(n, N) = \sum_{\{N_p\}} \omega(\{N_p\}) \tag{C.1}$$

where $\omega(\{N_p\}) = N!/\prod_{p=0}^{\min(n,2S)} N_p!$, subject to the conditions (B.2) and (B.3).

Although the magnon operators are Bose operators, they are not associated with an infinity of states in our treatment. Thus the probability distribution differs from the Planck distribution. We require to maximize $\omega(\{N_p\})$ for variation of N_p subject to the conditions (B.2) and (B.3). Using Lagrange's undetermined multiplier γ and μ, and for arbitrary variations $\mathrm{d}N_p$, we get

$$N_p = \mathrm{e}^{-\gamma-\mu p}. \tag{C.2}$$

This is valid for the maximum component $\omega(\{N_p\})$ for any n. Each set of p values has been considered separately. A consideration of temperature will enter later.

Furthermore, while n_{pj} is the number of magnons of spin p and in state j with energy ε_{pj}, one may observe the relations

$$\sum_{p=0}^{\min(n,2S)} n_{pj} = N_p, \qquad \sum_{p=0}^{\min(n,2S)} n_{pj}\varepsilon_{pj} = E_p, \tag{C.3}$$

and

$$\widetilde{\omega_p}(\{n_{pj}\}) = \frac{N_p!}{\prod_j n_{pj}!}.$$

The $\widetilde{\omega_p}$ terms constitute the components of maximum $\omega(\{N_p\})$. To create the temperature dependence, we require $\widetilde{\omega_p}(\{n_{pj}\})$ to be maximum for a fixed E_p. Thus

$$\mathrm{d}\ln \widetilde{\omega_p}(\{n_{pj}\}) = 0, \qquad \mathrm{d}E_p = 0. \tag{C.4}$$

Using Lagrange's undetermined multiplier β, we get for arbitrary variation of n_{pj}, the form $n_{pj} = N_p \exp[-\beta\varepsilon_{pj}]$. This finally yields the distribution

$$\frac{n_{pi}}{N} = \frac{\exp(-\mu p - \beta\varepsilon_{pi})}{\sum_{q=0}^{\min(n,2S)} \sum_{j\in q} \exp(-\mu q - \beta\varepsilon_{qj})}. \tag{C.5}$$

In the derivation given here, we have used the conditions $\mathrm{d}E_p = 0$ for each p that is stronger than the normally used condition $\mathrm{d}E = 0$ where $E = \sum_{p=0}^{\min(n,2S)} E_p$.

At first, the largest component of $W_S(n, N)$ is found for fixed n and N. This yields the infinite temperature result where all the states are *a priori* equally probable. For each type of spin states (for each site or for each magnon mode), the probability function for a specific N_p is maximized subject to the constraint of constant E_p. So each type of spin state constitutes a canonical ensemble. The final result is, of course, a grand canonical distribution function considering all types (p values). It now becomes trivially simple to show that $\beta = 1/k_\mathrm{B}T$ and μ is the chemical potential.

Appendix D. Use of $W_S(n, N)$ in sums

Here we inspect two types of summation involving the number of microstates for any general spin S, although the exact analytical function $W_S(n, N)$ is not known except for $S = 1/2$. These sums are often encountered in treatments of solid state physics. The sums considered are

$$\mathsf{S}_1(x, N) = \sum_{n=0}^{2NS} x^n W_S(n, N) \tag{D.1}$$

and

$$\mathsf{S}_2(x, N) = \sum_{n=0}^{2NS} nx^n W_S(n, N). \tag{D.2}$$

Of course, $\mathsf{S}_2(x, N) = x\ (\mathrm{d}\mathsf{S}_1\ (x, N)/\mathrm{d}x)$.

Using the regression property (B.7) we find

$$\mathsf{S}_1(x, N) = \left(\frac{1-x^{2S+1}}{1-x}\right)\mathsf{S}_1(x, N-1) + \sum_{n=1}^{2S}\left(\frac{1-x^{2S+1-n}}{1-x}\right)x^{2(N-1)S+n} \times W_S(2(N-1)S+n, N-1). \tag{D.3}$$

As $N \to \infty$, the second term on the right-hand side of (D.3) can be neglected. Also, $\mathsf{S}_1(x, 1) = (1-x^{2S+1})/(1-x)$. Therefore, for a general spin S, the $N \to \infty$ limit of S_1 is given by

$$\mathsf{S}_1(x, N) = \left(\frac{1-x^{2S+1}}{1-x}\right)^N. \tag{D.4}$$

Using this S_1, one finds the large N behavior

$$\mathsf{S}_2(x, N) = Nx\frac{(1-x^{2S+1})^{N-1}}{(1-x)^{N+1}}(2Sx^{2S+1} - (2S+1)x^{2S} + 1). \tag{D.5}$$

References

[1] Holstein T and Primakoff H 1940 *Phys. Rev.* **58** 1098

[2a] Soos Z G 1965 *J. Chem. Phys.* **43** 1121
Soos Z G and Hughes R G 1967 *J. Chem. Phys.* **46** 253
Silverstein A J and Soos Z G 1970 *J. Chem. Phys.* **53** 326

[2b] Fedders P A and Kommandeur J 1970 *J. Chem. Phys.* **52** 2014

[2c] Nagle J F and Bonner J C 1971 *J. Chem. Phys.* **54** 729

[2d] Lepine Y and Caille A 1977 *J. Chem. Phys.* **67** 5598

[2e] Klein D J 1982 *J. Chem. Phys.* **77** 3098
Cheranovski V O, Schmalz T G and Klein D J 1994 *J. Chem. Phys.* **101** 5841

[2f] Costas M E, Wang Z G and Gelbart W M 1992 *J. Chem. Phys.* **96** 2228

[2g] Ondrechen M J, Gozashti S and Wu X M 1992 *J. Chem. Phys.* **96** 3255
[2h] Kollmar C and Kahn O 1993 *J. Chem. Phys.* **98** 453
[2i] Cable J W 1981 *Phys. Rev.* B **23** 6168
[2j] Datta S N and Misra A 1999 *J. Chem. Phys.* **111** 9009
[3a] Bethe H A 1931 *Z. Phys.* **71** 205
[3b] Hulthén L 1938 *Arkiv Mat. Astron. Fys.* A **26** 1
[3c] Kasteleijn P W 1952 *Physica* **18** 104
[3d] Marshall W 1955 *Proc. R. Soc.* A **232** 48
[3e] Taketa H and Nakamura T 1956 *J. Phys. Soc. Japan* **11** 919
[4a] Bonner J C and Fisher M E 1964 *Phys. Rev.* **135** A640
[4b] Orbach R 1958 *Phys. Rev.* **112** 309
[4c] Huber D L 1973 *Phys. Rev.* B **8** 2124
[4d] Foo E-N and Bose S M 1974 *Phys. Rev.* B **9** 3944
[4e] Schlottmann P 1985 *Phys. Rev. Lett.* **54** 2131
[4f] Xiang T and Gehring G A 1993 *Phys. Rev.* B **48** 303
[5a] Dyson F J 1956 *Phys. Rev.* **102** 1217
[5b] Hanus J 1962 *Q. Prog. Rep. Solid State Mol. Theory Group* **43** 96
Hanus J 1962 *Q. Prog. Rep. Solid State Mol. Theory Group* **44** 38
Hanus J 1962 *Q. Prog. Rep. Solid State Mol. Theory Group* **46** 137
[5c] Wortis M 1963 *Phys. Rev.* **132** 85
[5d] Fukuda N and Wortis M 1963 *J. Phys. Chem. Solids* **24** 1675
[5e] Boyd R G and Callaway J 1965 *Phys. Rev.* **138** A1621
[5f] Majumdar C K 1969 *J. Math. Phys.* **10** 177
[5g] Majumdar C K 1970 *Phys. Rev.* B **1** 287
[5h] Ghosh D K and Mukhopadhyay G 1970 *J. Phys. C: Solid State Phys.* **3** 323
[5i] Kadolkar C, Ghosh D K and Sarma C R 1992 *J. Phys.: Condens. Matter* **4** 9651
[5j] Reser B I and Melnikov N B 2008 *J. Phys.: Condens. Matter* **20** 285205
[6] Kittel C 1963 *Quantum Theory of Solids* (New York: Wiley)
Kittel C 1996 *Introduction to Solid State Physics* (New York: Wiley)
[7] Datta S N and Panda A 2009 in preparation
[8] Bloch M 1962 *Phys. Rev. Lett.* **9** 286
[9a] Kubo R 1952 *Phys. Rev.* **87** 568
[9b] Anderson P W 1952 *Phys. Rev.* **86** 694
[9c] Anderson P W 1973 *Mater. Res. Bull.* **8** 153
[9d] Anderson P W, Baskaran G, Zou Z and Hsu T 1987 *Phys. Rev. Lett.* **58** 2790
[9e] Anderson P W and Morel P 1961 *Phys. Rev.* **123** 1911
[10] Dyson F J 1956 *Phys. Rev.* **102** 1217
[11] Weiss P 1907 *J. Physique* **6** 661
[12] Crangle J and Goodman G M 1971 *Proc. R. Soc.* A **321** 477
[13] Yosida K 1998 *Theory of Magnetism* 2nd edn (Heidelberg: Springer)
[14] Alda E, Bazán B, Mesa J L, Pizarro J L, Arriortua M I and Rojo T 2003 *J. Solid State Chem.* **173** 101
[15a] Domb C and Sykes M F 1962 *Phys. Rev.* **128** 168
[15b] Rushbrooke G S and Wood P S 1958 *Mod. Phys.* **1** 257
[16] Gammel J, Marshall W and Morgan L 1963 *Proc. R. Soc.* **275** 257
[17] Kouvel J S and Fisher M E 1964 *Phys. Rev.* **136** A1626
[18] Bloch F 1930 *Z. Phys.* **61** 206
Bloch F 1932 *Z. Phys.* **74** 295
[19] Weiss P and Forrer R 1926 *Ann. Phys., Lpz.* **5** 153
Weiss P and Forrer R 1929 *Ann. Phys., Lpz.* **12** 279